Journal of Solid State Chemistry 183 (2010) 1075–1082

Contents lists available at ScienceDirect

Journal of Solid State Chemistry

journal homepage: www.elsevier.com/locate/jssc

Hydrogen production from water decomposition by redox of Fe_2O_3 modified with single- or double-metal additives

Xiaojie Liu, Hui Wang *

Key Laboratory of Synthetic and Natural Functional Molecule Chemistry (Ministry of Education), College of Chemistry and Materials Science, Northwest University, Xi'an 710069, PR China

ARTICLE INFO

Article history:
Received 28 January 2010
Received in revised form
25 February 2010
Accepted 7 March 2010
Available online 15 March 2010

Keywords:
Hydrogen production
Fe_2O_3
Water decomposition
Mo or Mo–Zr additives

ABSTRACT

Iron oxide modified with single- or double-metal additives (Cr, Ni, Zr, Ag, Mo, Mo–Cr, Mo–Ni, Mo–Zr and Mo–Ag), which can store and supply pure hydrogen by reduction of iron oxide with hydrogen and subsequent oxidation of reduced iron oxide with steam (Fe_3O_4 (initial Fe_2O_3)+$4H_2 \leftrightarrow 3Fe+4H_2O$), were prepared by impregnation. Effects of various metal additives in the samples on hydrogen production were investigated by the above-repeated redox. All the samples with Mo additive exhibited a better redox performance than those without Mo, and the Mo–Zr additive in iron oxide was the best effective one enhancing hydrogen production from water decomposition. For Fe_2O_3–Mo–Zr, the average H_2 production temperature could be significantly decreased to 276 °C, the average H_2 formation rate could be increased to 360.9–461.1 μmol min^{-1} Fe-g^{-1} at operating temperature of 300 °C and the average storage capacity was up to 4.73 wt% in four cycles, an amount close to the IEA target.

1. Introduction

Hydrogen is an ideal energy carrier because of its high efficiency, zero emission and production from renewable biomass [1,2]. Thus, hydrogen has been recognized as a clean energy substitute for fossil fuels but has not been used yet. One of the major problems for the large-scale use of hydrogen is the difficulty of an efficient storage [3,4]. The present hydrogen storage technologies are mainly physical method such as pressurized gas and cryogenic liquid, and chemical one such as storing in various solid and liquid materials; however, the solid storage has been considered as the safest and most effective way [5]. Among the various candidates of hydrogen storage solid materials including metal hydrides, complex hydrides and carbon materials [6–15], none is capable of meeting the US Department of Energy (DOE) and International Energy Agency (IEA) cost and performance targets for use in transportation vehicles that is hydrogen storage capacity of 6.5 wt% (62 kg H_2/m^3) or 5 wt% (50 kg H_2/m^3) [16].

Recently, a new class of iron oxide solid material has attracted much attention because of their potential applications in hydrogen storage and production processes [17–22]. Otsuka et al. reported a new, simple, safe, inexpensive and environmentally compatible technology for the storage and supply of hydrogen to polymer electrolyte fuel cell (PEFC) vehicles by the redox reaction of Fe_3O_4 (or initial Fe_2O_3)+$4H_2 \leftrightarrow 3Fe+4H_2O$ [23]. First, Fe_3O_4 or initial Fe_2O_3 is reduced to active Fe by H_2 (hydrogen storage at reduction step 1), and then the active Fe (reduced iron oxide) is oxidized to Fe_3O_4 by H_2O vapor (hydrogen production at oxidation step 2). According to reaction 2, 1 mol of Fe reacts with H_2O can produce 1.33 mol of H_2, which corresponds to the theoretical amount of hydrogen being chemically stored (i.e., 4.8 wt% of Fe). This value is relatively higher than hydrogen storage capacities of the above-mentioned materials. Furthermore, the operating pressure of releasing H_2 is normal pressure and hydrogen is the only product. Despite the many advantages of the solid material, however, the utilization of iron oxide as a possible substitute for hydrogen storage material requires the solution of several problems related to hydrogen production, such as H_2 production rate at a low operating temperature, reversible cycle stability and hydrogen storage capacity.

2. Experimental section

2.1. Reagent and instrument

Fe_2O_3 (99.8%) was purchased from Bodi chemical company in Tianjin. $AgNO_3$ (99.8%), $Cr(NO_3)_3 \cdot 9H_2O$(99.0%) and $NiCl_2 \cdot 6H_2O$(98.0%) were purchased from Kerme company in Tianjin. $(NH_4)_6Mo_7O_{24} \cdot 4H_2O$(99.0%) and $ZrOCl_2 \cdot 8H_2O$(98.0%) were purchased from the Chemical company in Xi'an. Scanning electron microscopy (SEM, a Quanta 400 FEG instrument operated at 25 kV, Oxford INCA 350 detector) and X-ray diffraction (XRD, D/max-3c, Cu$K\alpha$, 50 kV, 300 mA, at room temperature in air) were used to characterize the morphologies, particle sizes and

* Corresponding author. Fax: +86 029 88303798.
E-mail address: huiwang@nwu.edu.cn (H. Wang).

0022-4596/$ - see front matter © 2010 Elsevier Inc. All rights reserved.
doi:10.1016/j.jssc.2010.03.017

compositions of the samples. The specific surface areas of the samples were measured with a surface area analyzer (JW-K) by the adsorption of N_2 at liquid N_2 temperature (BET method). WFSM-3012 evaluating device with a gas chromatogram (GC, SP-6890) designed by ourselves was used to evaluate the redox performances of the samples, including H_2 production temperature, H_2 production rate, hydrogen storage capacity and cyclic stability.

2.2. Sample preparation

The Fe_2O_3 samples with single- or double-metal additives were prepared by impregnating Fe_2O_3 powder with an aqueous solution containing metal cation additives. The amount of added single-metal cation (M) was adjusted to be 5 mol% of total metal cations (M/(Fe+M)=0.05), while those of double-metal cations were adjusted to be 5 (Mo) and 2.5 (M) mol% of total metal cations (Mo/(Fe+Mo+M)=0.05 and M/(Fe+Mo+M)=0.025), respectively. The Fe_2O_3 powder was directly impregnated into 250 ml beaker with 150 ml distilled water containing the corresponding metal cation additives (single-metal cation (M) or double-metal cations (Mo+M)) in the above proportion. Then, the beaker with an aqueous solution was heated on the magnetic force mixer with thermoelectric couple to control temperature at 95 °C and the aqueous solution containing the corresponding metal salt were stirred thoroughly until water in the solution were steamed away. Next, the impregnated sample was dried at 90 °C for 10 h and subsequently calcined in air at 500 °C for 15 h. Nine kinds of as-prepared Fe_2O_3 samples with various metal additives were denoted as Fe_2O_3–Zr, Fe_2O_3–Ni, Fe_2O_3–Mo, Fe_2O_3–Ag, Fe_2O_3–Cr, Fe_2O_3–Mo–Zr, Fe_2O_3–Mo–Ni, Fe_2O_3–Mo–Ag and Fe_2O_3–Mo–Cr, respectively. Fe_2O_3 and Fe_3O_4 without additives were denoted as Fe_2O_3-none and Fe_3O_4-none, respectively.

The degree of oxidation of the reduced samples (DO) was defined as the ratio of actual hydrogen production amount to the theoretical total hydrogen production amount:

$$DO = \frac{mol_{actualpH_2}\ (actual\ hydrogen\ mole\ produced\ at\ time\ t)}{mol_{totalpH_2}\ (total\ hydrogen\ mole\ produced\ after\ complete\ oxidation)}$$

2.3. Samples' evaluation

The redox performances of these samples were evaluated by the WFSM-3012 evaluating device. The evaluating process comprises two steps, i.e., hydrogen storage and production, in which the redox performances such as hydrogen production temperature, the cyclic stability and hydrogen storage capacity could be tested. First, the sample bed, into which the sample (around 0.2 g) was put, was heated to 500 °C at a heating rate of 4 °C min^{-1}, and meanwhile H_2 as reduced gas and Ar as carrier gas were injected into the bed to reduce iron oxide to active Fe. When the temperature of the bed reached 500 °C, this temperature was being kept until no consumption of hydrogen was detected by gas chromatograph (GC). Then, the oxidation of active Fe could be performed successively to produce H_2 by the 1:4 gas mixture of H_2O vapor and Ar with the flow rate of 50 ml min^{-1}, as the temperature of the sample bed was increased to 600 °C from room temperature at a heating rate of 4 °C min^{-1} and the temperature was kept until hydrogen was no longer analyzed by GC.

3. Results and discussions

3.1. Selection of initial material

Both Fe_2O_3 and Fe_3O_4 were able to serve as the starting material for hydrogen storage, from which the better one should be found out by the redox reaction. In order to achieve the goal, the redox performances of Fe_2O_3 obtained by direct purchase and Fe_3O_4 obtained by a co-precipitation method were investigated. Fig. 1 shows that the changes of H_2 formation rate vs. temperature and of

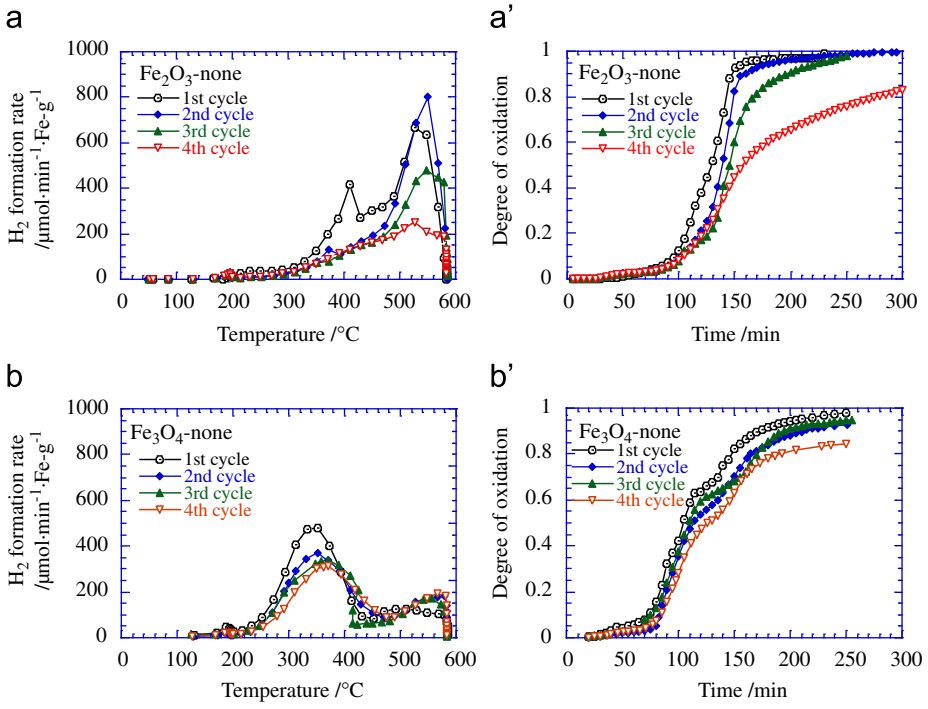

Fig. 1. Variations of H_2 formation rate vs. temperature, and of degree of oxidation vs. time in the re-oxidation of Fe_2O_3-none and Fe_3O_4-none in four redox cycles.

Table 1
The redox performances of Fe_2O_3-none and Fe_3O_4-none without additives.

Sample	Cycle	Peak temperature (°C)	H_2 formation temperature at the rate of 250 μmol min^{-1} Fe-g^{-1} (°C)	The rate of H_2 formation (μmol min^{-1} Fe-g^{-1})		The required time at the fixed DO (min)		H_2 (wt%)
				At peak temperature (°C)	At 300 (°C)	At 0.5000	At 0.7500	
Fe_2O_3-none	1st	528	380	668.3	43.5	128	140	4.88
	2nd	530	475	802.8	31.1	140	146	4.74
	3rd	549	491	478.6	25.9	145	160	4.64
	4th	528	525	249.3	29.8	158	240	3.94
Fe_3O_4-none	1st	353	288	480.1	323.8	104	139	4.69
	2nd	352	300	368.2	238.3	108	157	4.53
	3rd	370	310	339.3	224.9	112	162	4.48
	4th	371	321	312.7	157.8	125	168	4.05

DO vs. time for the Fe_2O_3-none and Fe_3O_4-none samples in four cycles. The corresponding data including the peak temperature, the rate of H_2 formation at peak temperature and 300 °C, the temperature of H_2 formation at the rate of 250 μmol min^{-1} Fe-g^{-1}, hydrogen storage capacity and the required time at a fixed DO were listed in Table 1.

As shown in Fig. 1a and b and listed in Table 1, the rates of H_2 formation for Fe_2O_3-none and Fe_3O_4-none at 300 °C were in the range of 25.9–43.5 and 157.8–323.8 μmol min^{-1} Fe-g^{-1} in four repeated cycles, respectively. It is clear that the H_2 production rate of Fe_3O_4-none was higher than that of Fe_2O_3-none at 300 °C. At the same time, the temperature of H_2 formation for Fe_3O_4-none at the rate of 250 μmol min^{-1} Fe-g^{-1} was much lower than that for Fe_2O_3-none. In addition, the average required time of Fe_3O_4-none at a fixed DO in four cycles was shorter than that of Fe_2O_3-none (see Fig. 1a′ and b′ and Table 1). Accordingly, it seems that Fe_3O_4-none should be preferred as the initial material for hydrogen storage compared with Fe_2O_3-none. However, hydrogen storage capacity, another important factor, for Fe_2O_3-none (4.69 wt%) was higher than that for Fe_3O_4-none (4.44 wt%) (Table 1), and Fe_2O_3 has other commercial advantages over Fe_3O_4, such as the direct purchase, abundant source and low cost. Therefore we chose the Fe_2O_3 powder as the starting material in the present work.

3.2. Effect of single- double-metal additives on hydrogen storage

Fig. 2 shows that the changes of H_2 formation rate vs. temperature for the samples with single-metal (Zr, Cr, Ag, Ni and Mo) and double-metal (Mo–Zr, Mo–Cr, Mo–Ag and Mo–Ni) additives, and the data related to hydrogen production were listed in Tables 2 and 3.

As shown in Fig. 2a–e and listed in Table 2, no matter what type of single metal added into Fe_2O_3 was, the redox performances of the samples were notably elevated. However, the effect of different metal on hydrogen production was different (Fig. 2a–e). E.g., the average temperatures of H_2 formation were 418, 396, 443, 501 and 276 °C for the Fe_2O_3–Zr, Fe_2O_3–Cr, Fe_2O_3–Ag, Fe_2O_3–Ni and Fe_2O_3–Mo samples in four repeated cycles, respectively. Obviously, the H_2 formation temperature of Fe_2O_3–Mo was much lower than that of the other samples. At a relatively low temperature of 300 °C, the H_2 formation rate of Fe_2O_3–Mo (487.5–453.1 μmol min^{-1} Fe-g^{-1}) was the highest among all of the samples with single metal, increased by about ten times compared with that of Fe_2O_3-none (43.5–29.8 μmol min^{-1} Fe-g^{-1}). Similarly, the average hydrogen storage capacities of Fe_2O_3–Zr, Fe_2O_3–Cr, Fe_2O_3–Ag, Fe_2O_3–Ni and Fe_2O_3–Mo were 4.54, 4.42, 4.64, 4.38 and 4.7 wt% in four redox cycles, respectively, indicating that Fe_2O_3–Mo also had the highest storage capacity, a near theoretical value of 4.8 wt%. Furthermore, the storage capacities of Fe_2O_3–Mo from the first to forth redox cycle (4.74, 4.63, 4.64 and 4.78 wt%) also showed a good cyclic stability for the sample. Based on the comparisons of all the modified Fe_2O_3 samples above, it is concluded that Mo additive had the most remarkable catalytic effect on improving hydrogen production. In addition, the kinetic curves in Fig. 2a–e show that the other metal additives also had a certain influence on improving the redox performances such as the cyclic stability. This may be due to the fact that the metal additives dispersed in the sample could effectively prevent the particle sintering of the sample. Therefore, it is necessary for us to further investigate the cooperative effect of Mo cation with other transition metal additive on improving hydrogen production.

As described above, Mo metal additive in iron oxide had the most effective influence on enhancing hydrogen production compared with other metals. So the cooperative effect of Mo metal with each one of the other four metals (Zr, Cr, Ag and Ni metal cations) as double-metal additives (Mo–Zr, Mo–Cr, Mo–Ag and Mo–Ni) in the sample on hydrogen production was also investigated. Comparing the kinetic curves and data in Fig. 2a′–e′ and Table 3 with those in Fig. 2a–e and Table 2, it is obvious that the double-metal additives (Mo–M) in the samples could improve hydrogen production more remarkably than the corresponding single-metal additives (M) except Mo additive. E.g., the average temperatures of H_2 formation for the Fe_2O_3–Mo–Zr, Fe_2O_3–Mo–Cr, Fe_2O_3–Mo–Ag and Fe_2O_3–Mo–Ni samples were 276, 275, 293 and 271 °C in four cycles, respectively, indicating that the temperatures were indeed lower than those for the corresponding samples with single-metal additives; the rates of H_2 formation at 300 °C for Fe_2O_3–Mo–Zr, Fe_2O_3–Mo–Cr, Fe_2O_3–Mo–Ag and Fe_2O_3–Mo–Ni were 360.9–461.1, 340.9–366.2, 168.5–343.4 and 516.2–369.8 μmol min^{-1} Fe-g^{-1} from the first to forth cycle, respectively, each of which is much higher than that of the samples with the corresponding single metal additive. This also indicates that these double-metal additives in the samples can enhance hydrogen production significantly. Furthermore, the average hydrogen storage capacities of Fe_2O_3–Mo–Zr, Fe_2O_3–Mo–Cr, Fe_2O_3–Mo–Ag and Fe_2O_3–Mo–Ni were 4.73, 4.61, 4.66 and 4.50 wt% in four cycles, respectively. It is apparent that the hydrogen storage capacity of Fe_2O_3–Mo–Zr (4.73 wt%), a close theoretical amount of 4.8 wt%, was the highest among all the samples tested in this work. It can be seen from Fig. 2a′–e′ that the kinetic curves for Fe_2O_3–Mo–Zr were overlapped more wonderfully than those for the others, showing that the Mo–Zr-modified sample had an excellent ability to preserve catalytic

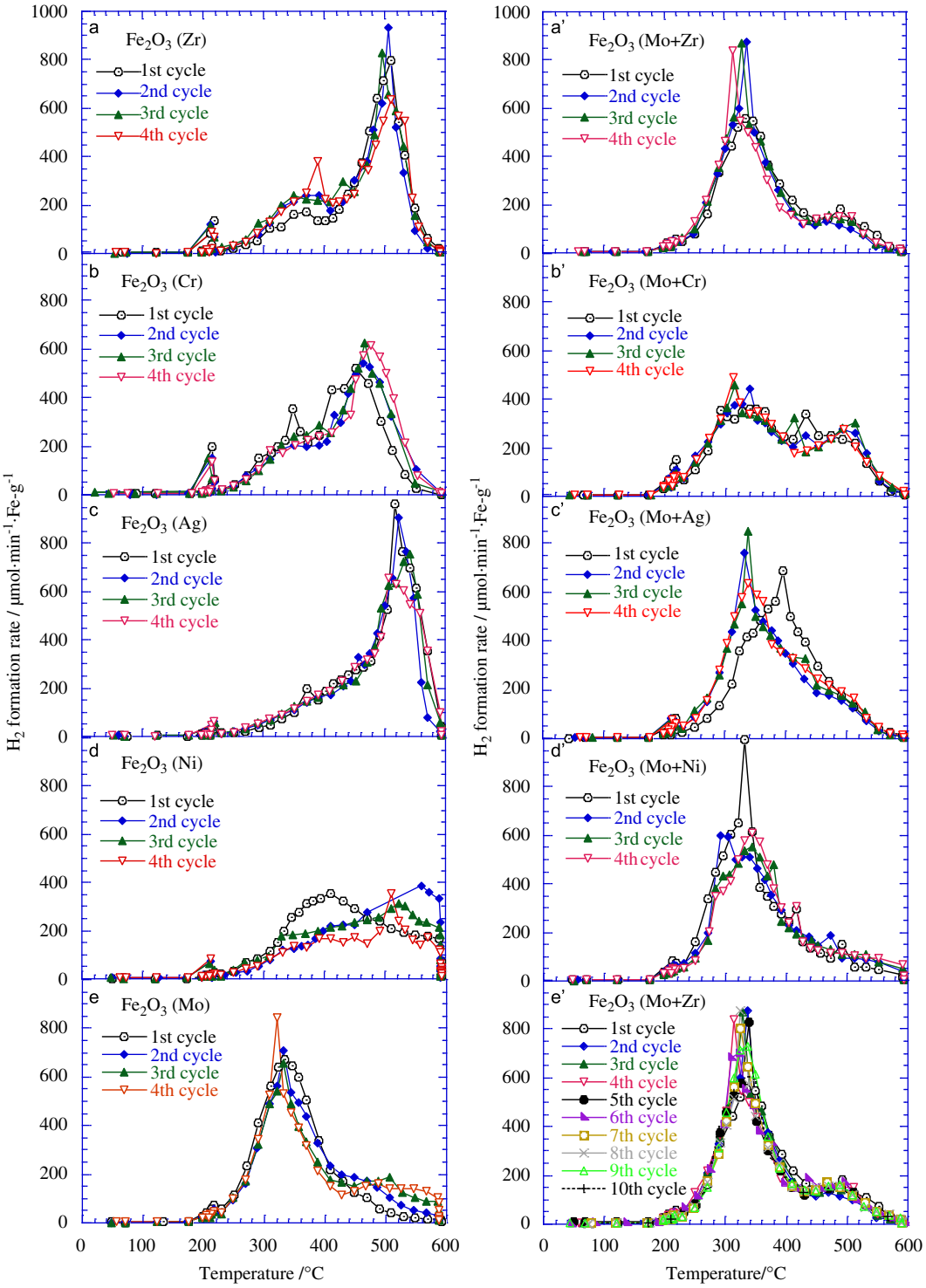

Fig. 2. Variations of H_2 formation rate vs. temperature for Fe_2O_3–Zr, –Cr, –Ag, –Ni, Mo and Fe_2O_3–Mo–M (Zr, Cr, Ag, Ni) in four redox cycles, and Fe_2O_3–Mo–Zr in ten cycles.

activity and cyclic stability. In the present work, the cycle times of Fe_2O_3–Mo–Zr were prolonged to ten in order to further observe the catalytic activity and cyclic stability. Obviously, the kinetic curves of Fe_2O_3–Mo–Zr in Fig. 2e′ were superposed perfectly in ten cycles, manifesting that the sample was not deactivated even after 10 cycles. According to the comparisons of all the Fe_2O_3 samples modified with single- and double-metal additives, it is concluded that all the samples with Mo additive show the good redox performances, and the Mo–Zr additive in the sample had the most remarkable role on improving hydrogen production.

3.3. *Characterization of the samples before and after redox*

To further understand the reason that the single- and double-metal additives in the modified Fe_2O_3 samples can enhance hydrogen production, SEM images, X-ray diffraction patterns and BET were used to characterize the morphologies, particle sizes and compositions of the samples before and after the redox. Figs. 3 and 4 depict the SEM images of the Fe_2O_3 modified with single- and double-metal additives before and after redox, respectively. From the SEM images of the samples in Figs. 3 and 4, it can be seen

Table 2
The redox performances of Fe_2O_3 modified with single metal (Zr, Cr, Ag, Ni and Mo).

Sample	Cycle	Peak temperature (°C)	H_2 formation temperature at 250 μmol min^{-1} Fe-g^{-1}	The rate of H_2 formation (μmol min^{-1} Fe-g^{-1})			H_2 (wt%)
				At peak temperature (°C)	At 300 (°C)	At 354 (°C)	
Fe_2O_3–Zr	1st	510	441	796.8	78.4	165.2	4.45
	2nd	508	444	932.3	98.7	218.7	4.43
	3rd	495	419	822.9	130.4	234.9	4.75
	4th	510	370	640.4	102.1	216.2	4.52
Fe_2O_3–Cr	1st	453	394	518.8	159.1	285.2	4.33
	2nd	464	406	543.5	125.0	204.1	4.34
	3rd	466	376	627.1	126.6	242.6	4.45
	4th	488	410	616.4	137.5	203.1	4.55
Fe_2O_3–Ag	1st	517	432	963.6	41.6	99.7	4.76
	2nd	523	449	911.5	42.8	121.4	4.44
	3rd	544	455	758.3	61.5	126.1	4.70
	4th	506	435	659.8	61.9	114.1	4.68
Fe_2O_3–Ni	1st	336	411	354.1	100.0	277.8	4.51
	2nd	403	560	386.7	60.78	170.2	4.70
	3rd	385	522	312.3	87.5	207.8	4.67
	4th	497	511	353.4	77.1	135.4	3.63
Fe_2O_3–Mo	1st	333	270	670.8	487.5	616.6	4.74
	2nd	333	279	704.2	416.6	500.0	4.63
	3rd	333	279	654.9	435.2	385.5	4.64
	4th	323	277	453.1	453.1	395.8	4.78

Table 3
The redox performances of Fe_2O_3 modified with double metals Mo+M (Zr, Cr, Ag and Ni).

Sample	Cycle	Peak temperature (°C)	H_2 formation temperature at 250 μmol min^{-1} Fe-g^{-1}	The rate of H_2 formation (μmol min^{-1} Fe-g^{-1})			H_2 (wt%)
				At peak temperature (°C)	At 300 (°C)	At 354 (°C)	
Fe_2O_3–Mo+Cr	1st	338	275	358.7	340.9	356.0	4.66
	2nd	340	277	441.7	331.6	312.5	4.62
	3rd	316	278	458.2	342.7	323.1	4.72
	4th	312	272	488.1	366.2	334.7	4.44
Fe_2O_3–Mo+Ag	1st	396	305	687.2	168.5	448.0	4.61
	2nd	332	285	756.8	350.3	523.0	4.65
	3rd	337	290	848.9	307.1	490.0	4.71
	4th	336	293	634.4	343.4	558.0	4.66
Fe_2O_3–Mo+Ni	1st	332	262	936.4	516.2	402.5	4.68
	2nd	291	274	565.2	562.5	427.1	4.53
	3rd	344	274	518.6	408.1	494.7	4.35
	4th	344	275	577.3	369.8	542.1	4.45
Fe_2O_3–Mo+Zr	1st	335	279	555.4	360.9	518.0	4.67
	2nd	338	276	875.3	396.1	439.0	4.74
	3rd	327	273	868.9	429.1	488.0	4.79
	4th	313	278	818.5	461.1	435.0	4.70
	5th	339	276	828.1	433.4	405.0	4.67
	6th	322	278	700.0	434.6	484.0	4.72
	7th	326	282	802.1	420.8	423.0	4.68
	8th	326	277	875.1	404.3	411.0	4.56
	9th	338	282	733.3	457.3	559.0	4.62
	10th	338	278	604.1	443.1	490.0	4.64

that the particles of all the samples after the redox existed sintering in a certain degree due to repeated cycle times at relatively high reaction temperature, but there were no obvious differences in particle size between the samples with double-metal additives before and after the redox except the Fe_2O_3–Mo–Zr sample. Furthermore, it can be seen from the SEM images in Fig. 3b and b′ that the particle size of the Fe_2O_3–Cr sample seems unchanged before and after the redox, but the sample still didn't show the good redox performances because of the low average H_2 production rate (137.05 μmol min^{-1} Fe-g^{-1}) at 300 °C and the high average H_2 production temperature (397 °C). It is also observed from Fig. 4a and a′ that the particles of the Fe_2O_3–Mo–Zr sample were sintered severely after 10 redox cycles, but the sample displayed the most excellent redox performances due to the lowest H_2 production temperature (276 °C). Accordingly, it is suggested that the change of particle size, i.e., whether the sample sintering or not, was not the key factor to decide the redox performances of the sample, but the type of metal additive in the sample, such as Mo metal, may be more important one to promote the production of hydrogen effectively.

From the conclusions obtained above, it is certain that Mo additive in the sample acted an important role on improving

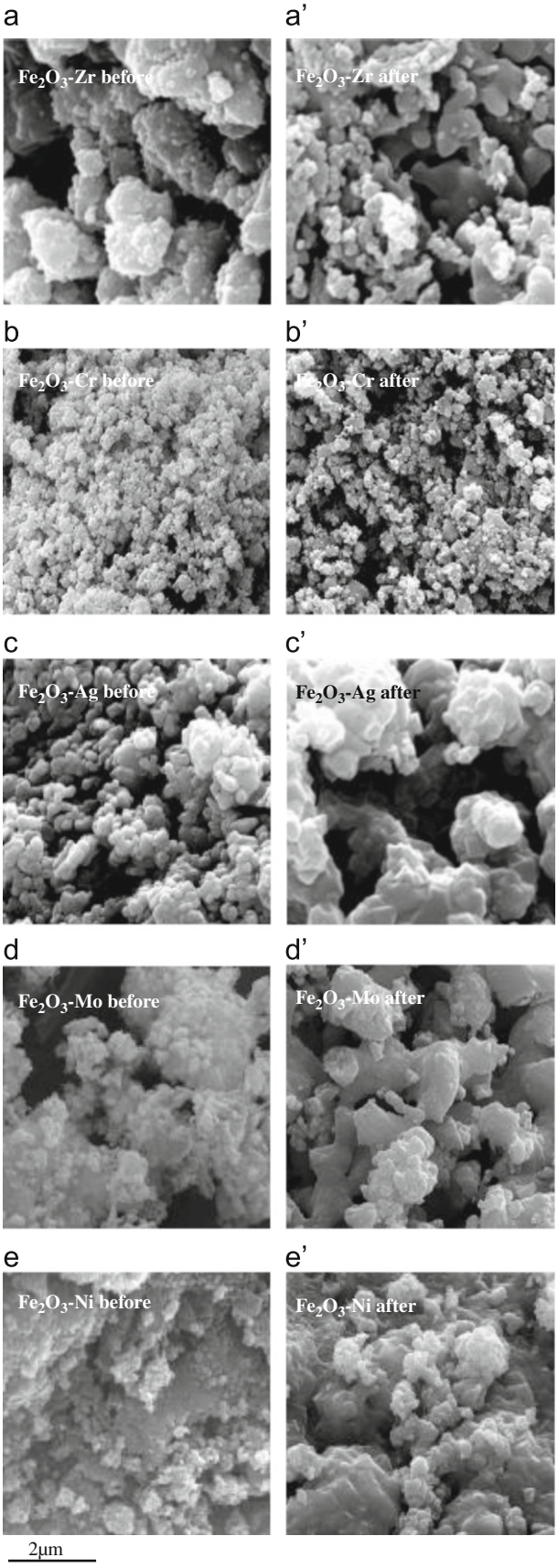

Fig. 3. SEM images of the Fe_2O_3 samples with single-metal additive before and after the redox.

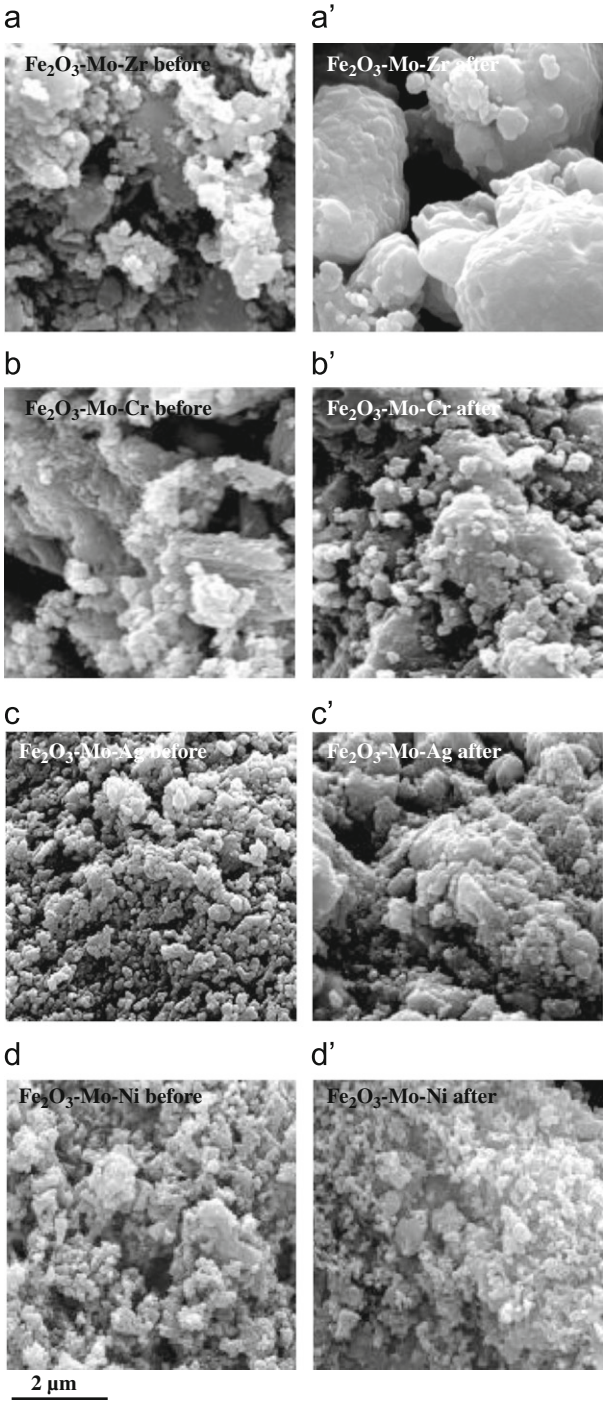

Fig. 4. SEM images of the Fe_2O_3 samples with double-metal additives before and after the redox.

hydrogen production, thus more attention were paid to the characterization of the samples with Mo additive. The reason for the Mo additive decreasing the H_2 formation temperature in a large degree might be just as assumed that the Mo cation took part in the redox reaction and further resulted in accelerating the reaction between active Fe and H_2O vapor, i.e., water decomposition reaction. This conclusion is the same as our previous experiment result [19], and will be further confirmed by the XRD results below.

The XRD results for the samples with Mo, Zr and Mo+Zr before and after the redox were shown in Fig. 5 and the standard XRD

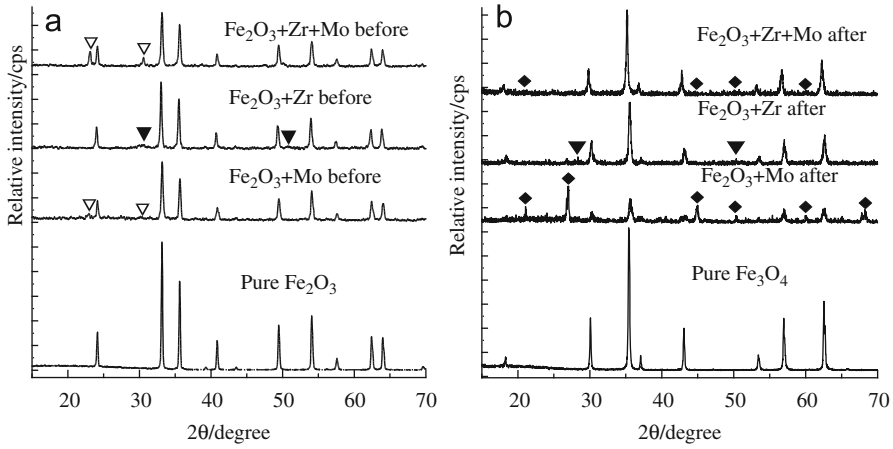

Fig. 5. XRD spectra of Fe_2O_3–Mo, Fe_2O_3–Zr and Fe_2O_3–Mo–Zr before (a) and after (b) the redox; pure Fe_2O_3 and Fe_3O_4 as reference standards: ▽, $Fe_2(MoO_4)_3$ ♦, $Fe_2Mo_3O_8$ and ▼, ZrO_2.

Table 4
BET surface areas of Fe_2O_3-none, Fe_2O_3–Mo and Fe_2O_3–Mo–Zr before and after the redox.

Sample	BET surface area of the fresh sample (m^2/g)	BET surface area of the sample after 4 cycles (m^2/g)	BET surface area of the sample after 10 cycles (m^2/g)	Ratio of BET surface area decrease after 4 cycles (m^2/g)
Fe_2O_3-none	3.96	0.16	–	0.96
Fe_2O_3–Mo	3.54	2.87	–	0.19
Fe_2O_3–Mo–Zr	13.67	8.24	2.64	0.40

spectra of pure Fe_2O_3 and Fe_3O_4 were used for comparison. Besides the main characteristic diffraction peaks assigned to Fe_2O_3 and Fe_3O_4, some other diffraction peaks due neither to Fe_2O_3 nor to Fe_3O_4 could also be observed for the Fe_2O_3–Mo, Fe_2O_3–Zr and Fe_2O_3–Mo–Zr samples before and after the redox cycle in Fig. 5a and b. E.g., for the samples before and after the redox cycle, two obvious diffraction peaks ascribed to $Fe_2(MoO_4)_3$ (JCPDS 35-0183) could be observed in Fig. 5a for Fe_2O_3–Mo–Zr and Fe_2O_3–Mo, while a few obvious peaks for Fe_2O_3–Mo and slight peaks for Fe_2O_3–Mo–Zr nearly in accordance with $Fe_2Mo_3O_8$ (JCPDS 74-1429) could be found in Fig. 5b. Two slight diffraction peaks ascribed to ZrO_2 (JCPDS 65-1022) could be found in Fe_2O_3–Zr before and after the cycle but did not exist in Fe_2O_3–Mo–Zr, which may be that the amount of Zr added in Fe_2O_3 was too small to be detected due to only amount of 2.5 mol% Zr cation in Fe_2O_3–Mo–Zr. Accordingly, it is concluded that the oxidation number of Mo that existed in the form of molybdate species varied from Mo^{6+} before the redox to Mo^{4+} after the redox, and the Zr additive in the form of ZrO_2 presented in its sample before and after the redox cycle. It is the valence change of Mo that prevented the particles of the samples from sintering. Meanwhile, based on our previous experimental result of Mo^{3+} existing in the reduced fresh sample and the present experiment, we consider that the following ionic reactions may take place: $2Mo^{6+}+3H_2 \rightarrow 2Mo^{3+}+6H^+$ (only for the reduction step of the fresh sample) and the subsequent reversible reaction of $2Mo^{3+}+H_2O \leftrightarrow 2Mo^{4+}+H_2+O^{2-}$ (for the oxidation step of the reduced iron oxide). It is the reversible change of $Mo^{3+} \leftrightarrow Mo^{4+}$ that accelerated the water decomposition and further resulted in the decrease of H_2 production temperature, which here was called as the catalytic effect of Mo catalysis. In addition to the Mo catalysis in Fe_2O_3–Mo–Zr, another reason for the Fe_2O_3–Mo–Zr sample having the best performances to produce hydrogen may be the assisted catalysis of Zr in Fe_2O_3–Mo–Zr due to the unchanged valence of Zr cation in the sample before and after the redox.

The specific surface areas of the samples were measured with a surface area analyzer by the adsorption of N_2 at liquid N_2 temperature (BET method). The detailed data of Fe_2O_3-none, Fe_2O_3–Mo, Fe_2O_3–Mo–Zr before and after the redox cycle were listed in Table 4. The data in Table 4 showed that BET specific surface areas for the cation-modified samples decreased a little compared with the none-modified Fe_2O_3 sample after four cycles, proving that the addition of foreign metals to Fe_2O_3 could effectively prevent the sintering of the particles. Whereas, with the cycle times rising to 10, the specific surface area of the Fe_2O_3–Mo–Zr sample changed from 8.24 after 4 cycles to 2.64 m^2/g after 10 cycles. With increasing cycle time, a large change of specific surface area did not cause the decrease of redox performances of Fe_2O_3–Mo–Zr, which also confirmed that the type of additive may be more important for improving the redox performances of the modified sample.

4. Conclusions

The redox performances of the modified Fe_2O_3 samples with single- or double-metal additives (Zr, Cr, Ag Mo and Ni; Mo–Zr, Mo–Cr, Mo–Ag and Mo–Ni) were investigated. Among all the additives in Fe_2O_3, the catalytic effect of Mo–Zr on hydrogen production was the most effective. The reason for it is that the addition of Mo to Fe_2O_3, on the one hand, could prevent the sintering of the particles effectively, and on the other hand, could promote the decomposition of water due to the valence change of Mo cation ($Mo^{3+} \leftrightarrow Mo^{4+}$) before and after the redox. E.g., Fe_2O_3–Mo–Zr exhibited the lowest H_2 production temperature (276 °C) at the rate of H_2 formation of 250 μmol min^{-1} Fe-g^{-1}, the highest rate of H_2 formation (360.9–461.1 μmol min^{-1} Fe-g^{-1}) from the first to fourth cycle at 300 °C, the best cyclic stability of hydrogen storage/release at operating temperature (no deactivation phenomenon after 10 cycles) and the high average capacity of hydrogen storage in four cycles (4.73 wt%).

Acknowledgments

The authors acknowledge the financial supports of the National Hi-Tech Research and Development Program (863) of China (no. 2007AA05Z116), the National Natural Science Foundation of China (nos. 20873099, 20673082), the Scientific Research Foundation for ROCS, SEM (no. 2006331), the Key Project of Science and Technology of Shaanxi Province (no. 2005k07-G2) and the Natural Science Foundation of Shaanxi Education Committee (no. 06JK167) the National Science Foundation for Fostering Talents in Basic Research (no. J0830417). The authors are also grateful to the State Key Laboratory of Continental Dynamics for the SEM measurements.

References

[1] L. Barreto, A. Makihira, K. Riahi, Int. J. Hydrogen Energy 28 (2003) 267.
[2] I. Dincer, Int. J. Hydrogen Energy 27 (2002) 265.
[3] M. Felderhoff, C. Weidenthaler, R. Helmolt, U. Eberle, Phys. Chem. Chem. Phys. 9 (2007) 2643.
[4] D.K. Ross, Vacuum 80 (2006) 1084.
[5] B. Sakintuna, F. Lamari-Darkrim, M. Hirscher, Int. J. Hydrogen Energy 32 (2007) 1121.
[6] J.M. Yan, X.B. Zhang, S. Han, H. Shioyama, Q. Xu, Angew. Chem. Int. Ed. 47 (2008) 2287.
[7] Z. Xiong, G. Wu, J. Hu, Adv. Mater. 16 (2004) 1522.
[8] G. Mpourmpakis, E. Tylianakis, G.E. Froudakis, Nano Lett. 7 (2007) 1893.
[9] H.M. Cheng, Q.H. Yang, C. Liu, Carbon 39 (2001) 1447.
[10] H. Shao, H. Xu, Y. Wang, X. Li, J. Solid State Chem. 177 (2004) 3626.
[11] A.M. Seayad, D.M. Antonelli, Adv. Mater. 16 (2004) 765.
[12] L. Zhou, Renew. Sust. Energy Rev. 9 (2005) 395.
[13] M. Sahlberg, C. Zlotea, P. Moretto, Y. Andersson, J. Solid State Chem. 182 (2009) 1833.
[14] H. Shao, Y. Wang, H. Xu, X. Li, J. Solid State Chem. 178 (2005) 2211.
[15] L. Zhou, Y. Zhou, Y. Sun, Int. J. Hydrogen Energy 29 (2004) 319.
[16] A. Züttel, Mater. Today 6 (2003) 24.
[17] K. Otsuka, C. Yamada, T. Kaburagi, S. Takenaka, Int. J. Hydrogen Energy 28 (2003) 335.
[18] H. Wang, S. Takenaka, K. Otsuka, Int. J. Hydrogen Energy 31 (2006) 1732.
[19] H. Wang, G. Wang, X. Wang, J. Bai, J. Phys. Chem. C 112 (2008) 5679.
[20] S. Takenaka, T. Kaburagi, C. Yamada, K. Nomura, K. Otsuka, J. Catal. 228 (2004) 66.
[21] V. Hacker, R. Vallant, M. Thaler, Ind. Eng. Chem. Res. 46 (2007) 8993.
[22] J.C. Ryu, D.H. Lee, K.S. Kang, C.S. Park, J.W. Kim, Y.H. Kim, J. Ind. Eng. Chem. 14 (2008) 252.
[23] K. Otsuka, T. Kaburagi, C. Yamada, S. Takenaka, J. Power Sources 122 (2003) 111.